Nonaxial octupole deformations in light $N=Z$ nuclei at high spins

Takeshi Tanaka and Rashid G. Nazmitdinov
Bogoliubov Laboratory of Theoretical Physics, Joint Institute for Nuclear Research, RU-141980 Dubna, Moscow Region, Russia

Kazuo Iwasawa
Information Processing Center, Hiroshima University, Hiroshima 739-8526, Japan

(Received 5 April 2000; published 14 February 2001)

High spin states of ^{32}S and ^{56}Ni are investigated by means of the cranking Hartree-Fock method with the Gogny interaction without imposing a restriction on the axial reflection symmetry. It is found that a nonaxial octupole deformation of the Y_{31} type becomes important in the yrast states of ^{32}S. A similar effect is predicted for the nucleus ^{56}Ni.

DOI: 10.1103/PhysRevC.63.034309 PACS number(s): 21.60.Jz, 21.10.Re, 27.30.+t, 27.40.+z

I. INTRODUCTION

One of the most important concepts in the many-body theory of finite Fermi systems is the mean field approach. Many phenomena observed in nuclei can be explained within this approach by means of a spontaneous symmetry breaking mechanism. As a result, we obtain a mean field solution that does not obey symmetries of the original many-body Hamiltonian [1,2]. For instance, a spontaneous breaking of the spherical symmetry for a nucleus with a partially filled highest shell gives rise to a deformed shape. Coriolis and centrifugal forces may cause a similar effect for a nucleus that has a near spherical shape in the ground state. In particular, a strong coupling of normal and intruder states near the Fermi surface at large rotational frequencies can lead to a superdeformed or to an octupole deformed shape for certain combinations of protons and neutrons [3]. The most practical way for the analysis of nuclear shapes is a phenomenological macroscopic-microscopic method. This approach combines the liquid drop model describing the macroscopic (bulk) properties of nuclear matter and the Strutinsky shell correction method providing the description of quantum shell effects of phenomenological mean field potentials [2]. The more fundamental approach is based on self-consistent Hartree-Fock (HF) calculations, once a particular choice of nucleon-nucleon interaction has been made. A commonly used internucleon force is that of Skyrme. Although the HF +Skyrme approach describes major features of nuclei quite well, it does not completely take the pairing correlations into account. In addition, various sets of parameters for Skyrme forces may not provide a definite answer in some cases. The Hartree-Fock-Bogoliubov (HFB) method with the Gogny forces resolves these problems quite effectively. Furthermore, it has the same predictive power as the macroscopic-microscopic method [4].

In recent years, many experimental and theoretical efforts have been devoted to the analysis of superdeformed (SD) bands in different mass regions [3,5–8]. On the other hand, the study of octupole degrees of freedom is also a topical subject in the nuclear structure physics [9,10]. It turns out that octupole deformations are significant for superdeformed nuclei as well as for normal-deformed (ND) ones. Most of these studies were restricted to the axial octupole deformation proportional to the Y_{30} term in the octupole family. The reason for this is primarily computational complications arising as a result of the extra degree of freedom introduced by nonaxial octupole deformations. However, during the last few years, some remarkable results have been reported. It was found that Y_{31} and Y_{32} components resulted in the lowest energy octupole vibrations for oblate and prolate superdeformed shapes and therefore could be essential for octupole instability [11,12,9]. Analysis based on the generator-coordinate method with the Skyrme effective interaction [13] confirmed that octupole excitations with $K=0$ and 2 could be strong for nonrotating SD nuclei in the Pb-Hg region. Calculations by the macroscopic-microscopic method with the Woods-Saxon potential predicted the importance of the banana-type Y_{31} deformation for highly deformed nuclei [14], while the Y_{32} deformation was found to be important in the ^{222}Ra nucleus [15]. The self-consistent HF+Skyrme calculations [16] suggest that the oblate states in nuclei with $A\sim 80$ are soft against the Y_{33} deformation in the ground states. The self-consistent cranking HF+Skyrme approach [17] predicts that the Y_{31} deformation is important for a correct description of the yrast band of ^{32}S. Moreover, the study of octupole deformations sheds light on the interplay between a classical chaos and a quantum spectrum of finite Fermi systems [18–20]. In the present paper, guided by the results of [21], we analyze how symmetries break at high spins in the cranking HFB approach with the Gogny interaction. In accordance with the octupole instability suggested at particle number $N=16$ and 28 [21], we choose two $N=Z$ nuclei, viz. ^{32}S and ^{56}Ni. In Sec. II, we review the main features of our model. The discussion of main results is presented in Sec. III and the conclusion in Sec. IV.

II. THE MODEL

The present self-consistent cranking HFB calculations have been performed with the effective Gogny D1S interaction [22–25]. This interaction provides a good description of many nuclear properties over the nuclide chart, e.g., ground state energies, odd-even energy differences, electron scattering data [23], and fission barriers [25]. Also, a good description is obtained for bulk properties of rotating nuclei in the actinide region [26], mercury region [27], and *fp*-shell region [28]. Our numerical code has been used for the analysis of microscopic dynamics in light rotating nuclei [29–31]. In these calculations, however, the signature symmetry was

conserved (see a discussion about different symmetries in rotating nuclei in [10,32]). The present calculations are performed without assuming the axial and signature symmetries *a priori*. In addition, our Hamiltonian includes the Coulomb interaction and the center of mass correction up to the exchange terms exactly.

The z axis is taken as a rotational axis in our code. To save the CPU time in numerical calculations, we impose the $\hat{P}e^{-i\pi\hat{J}_z}$ (z-simplex) and the $\hat{P}e^{-i\pi\hat{J}_y}\hat{\tau}$ ($\hat{S}_y^T$) symmetries [32], where $\hat{P}$ is the parity operator, $e^{-i\pi\hat{J}_i}$ is the rotation operator around the i axis ($i=y,z$) by angle π, and $\hat{\tau}$ is the time-reversal operator. Due to the z-simplex and $\hat{S}_y^T$ symmetries, the mass asymmetry of a nucleus is allowed only along the x axis. Thus, we solve numerically the following cranking HFB equations:

$$\delta\langle\phi(\omega)|\hat{H}-\lambda_p\hat{Z}-\lambda_n\hat{N}-\omega\hat{J}_z + \mu_x\langle\phi(\omega)|\hat{x}|\phi(\omega)\rangle\hat{x}|\phi(\omega)\rangle=0, \quad (1a)$$

$$\langle\phi(\omega)|\hat{Z}|\phi(\omega)\rangle=Z,\ \ \langle\phi(\omega)|\hat{N}|\phi(\omega)\rangle=N, \quad (1b)$$

$$\langle\phi(\omega)|\hat{J}_z|\phi(\omega)\rangle=I, \quad (1c)$$

$$\langle\phi(\omega)|\hat{x}|\phi(\omega)\rangle=0, \quad (1d)$$

where the Lagrange multipliers λ_p and λ_n are the chemical potentials of proton and neutron fields, respectively (the operators $\hat{Z}$ and $\hat{N}$ are proton and neutron number operators); the Lagrange multiplier ω is the angular frequency of a collective rotation around the z axis and $\hat{J}_z$ is the z component of the angular momentum operator $\hat{\boldsymbol{J}}$. To keep the center of mass motion fixed, we also impose the quadrupole constraint operator $\mu_x\langle\phi(\omega)|\hat{x}|\phi(\omega)\rangle\hat{x}$ [33] on the Routhian $\hat{R}=\hat{H}-\lambda_p\hat{Z}-\lambda_n\hat{N}-\omega\hat{J}_z$ in the x-axis direction.

The quasiparticle (qp) operators

$$\hat{\alpha}_i^\dagger=\sum_k U_{ki}\hat{c}_k^\dagger+V_{ki}\hat{c}_k, \quad (2)$$

where the state $|k\rangle$ is a single-particle basis state, obey the equation of motion

$$[\hat{R},\hat{\alpha}_i^\dagger]=\epsilon_i(\omega)\hat{\alpha}_i^\dagger \quad (3)$$

which defines the quasiparticle energies $\epsilon_i(\omega)$ and quasiparticle amplitudes U_{ki} and V_{ki} as functions of the rotational frequency ω.

We choose the y axis as the quantization axis of deformation. Consequently, the quadrupole, β_2 and γ, and octupole, β_{3m}, deformation parameters are defined as

$$\beta_2\cos\gamma\equiv\frac{4\pi}{5}\frac{\langle r^2Y_{20}(\theta,\varphi)\rangle}{AR_0^2}=\sqrt{\frac{\pi}{5}}\frac{\langle(3y^2-r^2)\rangle}{AR_0^2}, \quad (4)$$

$$\beta_2\sin\gamma\equiv\frac{4\pi}{5}\frac{\langle r^2(Y_{22}(\theta,\varphi)+Y_{2-2}(\theta,\varphi))\rangle}{\sqrt{2}AR_0^2}, = \sqrt{\frac{3\pi}{5}}\frac{\langle(x^2-z^2)\rangle}{AR_0^2}, \quad (5)$$

$$\beta_{30}\equiv\frac{4\pi}{3}\frac{\langle r^3Y_{30}(\theta,\varphi)\rangle}{AR_0^3}=\sqrt{\frac{7\pi}{9}}\frac{\langle y(5y^2-3r^2)\rangle}{AR_0^3}, \quad (6)$$

$$\beta_{31}\equiv\frac{4\pi}{3}\frac{\langle r^3[Y_{31}(\theta,\varphi)-Y_{3-1}(\theta,\varphi)]\rangle}{\sqrt{2}AR_0^3}, = -\sqrt{\frac{21\pi}{18}}\frac{\langle x(5y^2-r^2)\rangle}{AR_0^3}, \quad (7)$$

$$\beta_{32}\equiv\frac{4\pi}{3}\frac{\langle r^3[Y_{32}(\theta,\varphi)+Y_{3-2}(\theta,\varphi)]\rangle}{\sqrt{2}AR_0^3}, = \sqrt{\frac{105\pi}{9}}\frac{\langle y(x^2-z^2)\rangle}{AR_0^3}, \quad (8)$$

$$\beta_{33}\equiv\frac{4\pi}{3}\frac{\langle r^3[Y_{33}(\theta,\varphi)-Y_{3-3}(\theta,\varphi)]\rangle}{\sqrt{2}AR_0^3}, = -\sqrt{\frac{35\pi}{18}}\frac{\langle x(x^2-3z^2)\rangle}{AR_0^3}, \quad (9)$$

where (r,θ,φ) are spherical coordinates related to the Cartesian coordinates in the rotating frame (x,y,z) as

$$(x,y,z)\equiv(r\sin\theta\cos\varphi, r\cos\theta, r\sin\theta\sin\varphi). \quad (10)$$

All deformations proportional to the odd power of the y coordinate are forbidden in our code due to the $\hat{S}_y^T$ symmetry. Since β_{30} and β_{32} are proportional to the odd y^n terms, we use β_{31} and β_{33} to represent the degree of the nonaxial octupole deformation, when the y axis is the largest axis of a prolate nucleus. We recall that according to Ref. [21] we should expect strong nonaxial octupole deformations for ^{32}S and ^{56}Ni. Notice that the octupole deformation with a mass asymmetry like a pear shape is also represented by the combination of β_{31} and β_{33} when the x axis is the largest axis of a prolate nucleus: $\beta_{30}^x=\sqrt{6}/4\beta_{31}-\sqrt{10}/4\beta_{33}$. The s.p. wave functions have been expanded in a three-dimensional harmonic oscillator basis up to the principal quantum number $N=8$ for ^{32}S and up to $N=10$ for ^{56}Ni. The basis has been symmetrized with respect to the z-simplex operation, and eigenfunctions are eigenstates of the $\hat{S}_y^T$ operator (the Goodman basis [34]). Since the ground state shapes of the chosen nuclei are a normal-deformed one for ^{32}S and a spherical one for ^{56}Ni, we use a spherical Cartesian basis with the same range parameters of the Hermite polynomials for all axes. The range parameters have been optimized to reproduce the largest binding energy of each ground state. The same parameters have been used for all configurations discussed be-

low. The variation of the range parameters may lower the binding energy of an excited band, however, it could lead to the effective mixing of different configurations. On the other hand, the use of the fixed range parameters allows one to trace the evolution of the ground state configuration at different rotational frequencies. In addition, it makes transparent the single-particle level-crossing and simplifies the analysis related to a parity mixing discussed below. It is well known that for increasing shell number the optimal parameters change and then become rather stable [33]. The good agreement between our results and those obtained with much larger basis (see below) gives the reliability to our procedure.

To understand the relation between s.p. degrees of freedom and collective effects due to the rotation, we calculate three moments of inertia, the static moment of inertia $\mathcal{J}^{(1)}(\omega)\equiv I/\omega$, the dynamical moment of inertia $\mathcal{J}^{(2)}(\omega)\equiv dI/d\omega$, and the Inglis-Belyaev (IB) moment of inertia

$$\mathcal{J}_{\rm IB}(\omega)=2\sum_{i>j}\frac{|J_{ij}(\omega)|^2}{\epsilon_i(\omega)+\epsilon_j(\omega)}. \tag{11}$$

Here $J_{ij}(\omega)$ is a matrix element of the angular momentum operator $\hat{J}_z$

$$J_{ij}(\omega)=\langle\phi(\omega)|[\hat{\alpha}_j\hat{\alpha}_i,\hat{J}_z]|\phi(\omega)\rangle. \tag{12}$$

Since the angular momentum $I=\omega\mathcal{J}^{(1)}(\omega)$, the static and dynamical moments of inertia are not independent

$$\mathcal{J}^{(2)}(\omega)=\mathcal{J}^{(1)}(\omega)+\omega\frac{d\mathcal{J}^{(1)}(\omega)}{d\omega}. \tag{13}$$

As a consequence, the dynamical moment of inertia $\mathcal{J}^{(2)}(\omega)$ is very sensitive to structural rearrangements in the underlying nuclear structure like level crossings and shift in deformations. On the other hand, at a small rotational frequency, the total moment of inertia can be approximated as [35]

$$\mathcal{J}=\mathcal{J}_{\rm IB}+\mathcal{J}_{\rm M}+\sum_i\frac{\partial I}{\partial\beta_i}\frac{\partial\beta_i}{\partial\omega}. \tag{14}$$

The first term, $\mathcal{J}_{\rm IB}$, neglects a residual two-body interaction between quasiparticles. The second term $\mathcal{J}_{\rm M}$ is a Migdal moment of inertia, [36], resulting from the effect of rotation on the residual two-body interaction and, in particular, on the pairing interaction. The third term describes the variation of the self-consistent mean field, namely, the change of deformations under rotation. Although the calculation of the Migdal moment of inertia is a tractable task for simple separable forces [37], it is a nontrivial problem for density dependent realistic nonseparable interactions. Notice, that all three terms in Eq. (14) are included into the Thouless-Valatin moment of inertia [38] which can be calculated, for example, in the random phase approximation. In our analysis, the Thouless-Valatin moment of inertia is approximated by the dynamical moment of inertia $\mathcal{J}^{(2)}$. The rotation influences quasiparticle (single-particle) wave functions which define the density dependent two-body interaction. Consequently, it leads to a rearrangement of the two-body interaction and affects the $\mathcal{J}^{(2)}$. We also use the quantity $\mathcal{J}^{(2)}-\mathcal{J}_{\rm IB}$ to analyze the correlation between the $\mathcal{J}^{(2)}$ and structural changes of the self-consistent mean field (see below). In addition, we analyze different contributions to the IB moment of inertia, Eq. (11),

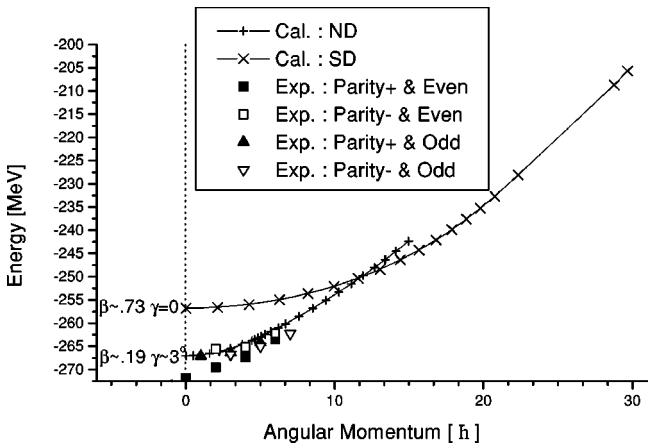

FIG. 1. The total binding energy in ^{32}S as a function of the angular momentum. The calculated points indicated by symbols + and × for ND and SD states, respectively, are connected by solid lines. Experimental values for states with different parities and spins are indicated by symbols: filled square is used for the positive parity and even values of I; open square is used for the negative parity and even values of I; filled triangle is used for the positive parity and odd values of I; open triangle is used for the negative parity and odd values of I. The experimental values of the total binding energy and excited levels from Refs. [39,40], respectively. The values of the quadrupole deformations β_2 and γ are given for each band at $I=0$.

$$\mathcal{J}_{\rm IB}(\omega)=\sum_{\tau,s}\mathcal{J}_{\tau,s}(\omega)\equiv\mathcal{J}_{p,+1}(\omega)+\mathcal{J}_{p,-1}(\omega)+\mathcal{J}_{n,+1}(\omega)+\mathcal{J}_{n,-1}(\omega), \tag{15}$$

where (τ,s) denote the isospin $(\tau=p,n)$ and the z-simplex quantum number $(s=\pm1$ characterizing different subspaces), respectively. The comparison of different components of $\mathcal{J}_{\rm IB}(\omega)$ could provide the information about the subspace in which the qp degrees of freedom mainly affect the bulk properties of the nuclei.

The cranking HFB equations (1a) are solved in an iterative way. As the convergence condition for each HFB state, we impose the condition

$$\sum_i|\epsilon_i^{(n)}(\omega)-\epsilon_i^{(n-1)}(\omega)|\leqslant 0.1[\text{keV}], \tag{16}$$

where n is the number of iterations in the course of solving the cranking HFB equations.

III. RESULTS AND DISCUSSION

A. ^{32}S

The results for the yrast line states and deformations as functions of the rotational frequency are presented in Figs. 1

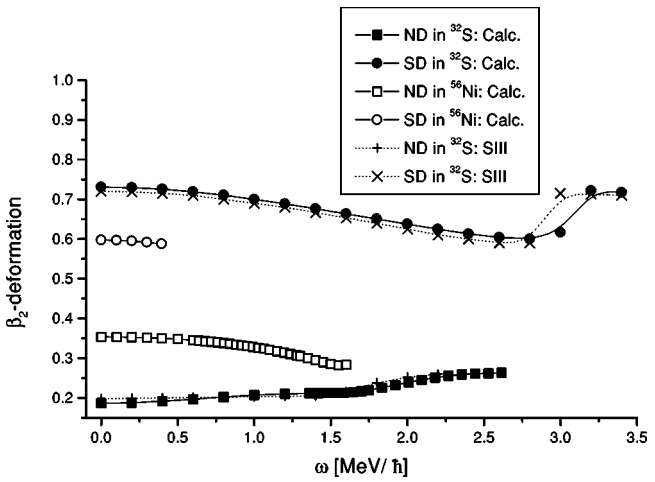

FIG. 2. β_2 deformation in ^{32}S and ^{56}Ni as a function of the rotational frequency ω. The following symbols are used: filled square and filled circle are used for ND and SD states, respectively, for ^{32}S; open square and open circle are used for ND and SD states, respectively, for ^{56}Ni; + and × are used for the results of calculations with the Skyrme III interaction [17].

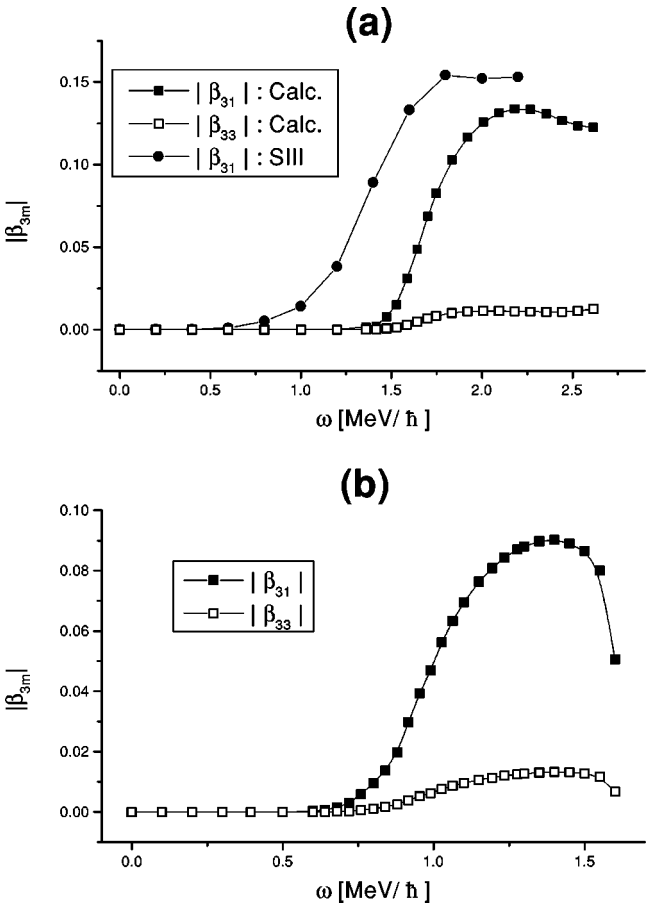

FIG. 3. The nonaxial octupole deformation: (a) in the ND yrast band of ^{32}S and (b) in the ND excited band of ^{56}Ni—as a function of the rotational frequency ω. The calculated values connected by solid lines are indicated by symbols: filled square is used for $|\beta_{31}|$; open square is used for $|\beta_{33}|$. SIII means the results of Ref. [17].

and 2. We found that the contribution from the pairing interaction terms to the total binding energy is almost negligible. The energy gaps between qp energies near the Fermi energies are large, about 4 MeV, both in the proton and neutron fields. Therefore, the calculations for the ND and SD bands have been done within the cranking HF approximation with the same parameter set as for the HFB calculations. Although there are differences in details between our calculations and those with Skyrme forces [17], our main results for the ND and SD bands are similar. In Fig. 2 one can see a good agreement between our results and ones from Ref. [17] for the evolution of β_2—deformations in the ND and SD bands. However, in our calculations with eight shells the excitation energy of the SD minimum relative to the ground state is 10.2 MeV in comparison with 12 MeV from Ref. [17]. Calculations with ten shells get reduced by 100 KeV ($\sim$1% effect) the excitation energy of the SD minimum. It is slightly different from the results of the HFB calculations of Rodriguez-Guzman, Egido, and Robledo [41] who, using the Gogny interaction as well, obtained 9.85 MeV with ten shells and 9.54 MeV with 18 shells. They found similar deformations for the ground state and SD HFB minima ($\beta_2=0.19$ and $\beta_2=0.73$, respectively). However, our estimation for the ground state binding energy is lower for ^{32}S than in [41] (-267.03 MeV compared to -261 MeV), since the Coulomb exchange term has been included self-consistently in our model. The ground state energy becomes -260.7 MeV and -261.0 MeV with eight and ten shells, respectively, without the contribution of the Coulomb exchange term. Similar calculations with 10 shells give 9.9 MeV for the excitation energy of the SD minimum. These results are in an excellent agreement with the HFB calculations [41] in which the Coulomb exchange term was neglected. In order to improve the results the authors of [41] used the angular momentum projected generator method (AMP-GCM) and obtained only the -2.5 MeV shift with respect to the HFB minimum [the binding energy becomes -263.5 MeV, see Fig. 2(a) in [41]]. Taking into account the Coulomb exchange energy in the AMP-GCM calculations [41], the additional shift -7.37 MeV has been obtained and the ground state binding energy becomes -270.87 MeV. All these facts confirm the importance of the Coulomb exchange term which is usually neglected in most HFB calculations due to its complication (see also discussion in Ref. [42]). Except for the binding energy, our results are also consistent with those of SLy4-HF calculations [43], in which the β deformations are $\beta_2=0.16$ and $\beta_2=0.7$ in the ground state and SD minimum state, respectively. The SD band becomes the yrast one for $I\geqslant 12\hbar$. Since we concentrate our analysis upon the octupole instability near the transition region from the ND band to the SD band, the description of the SD band is good enough for our purposes. In comparison with the results of the Skyrme III calculations [17], the finite values of the nonaxial octupole deformation Y_{31} in the ND yrast band are obtained at larger rotational frequency $\omega\geqslant 1.5$ [MeV/$\hbar$] in our approach. As is seen in Fig. 3(a), the value of the nonaxial octupole deformation $|\beta_{31}|$ increases suddenly at $\omega \sim 1.5$ [MeV/$\hbar$], where the pseudo level-crossing occurs between s.p. orbits in the subspaces with $s=+1$ [Fig. 4(a)],

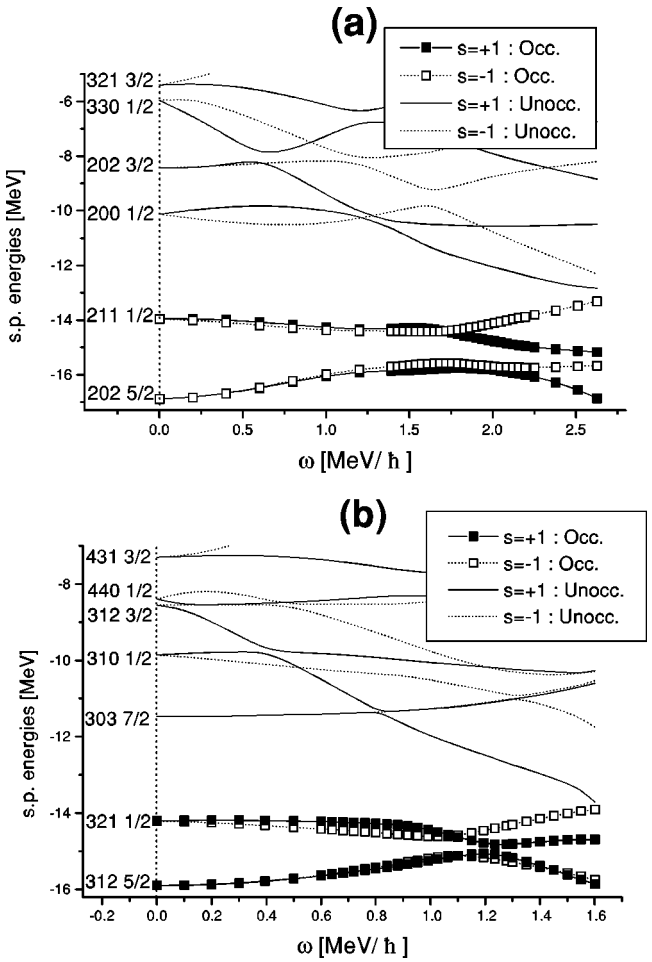

FIG. 4. Neutron single-particle energies near the Fermi surface versus the rotational frequency ω: (a) in ^{32}S and (b) in ^{56}Ni. The occupied states with different simplex quantum number s connected by lines are indicated by symbols: filled square and open square are used for the $s=+1$ and $s=-1$ states, respectively. The unoccupied states with the simplex $s=+1$ and $s=-1$ are connected by solid and dotted lines, respectively.

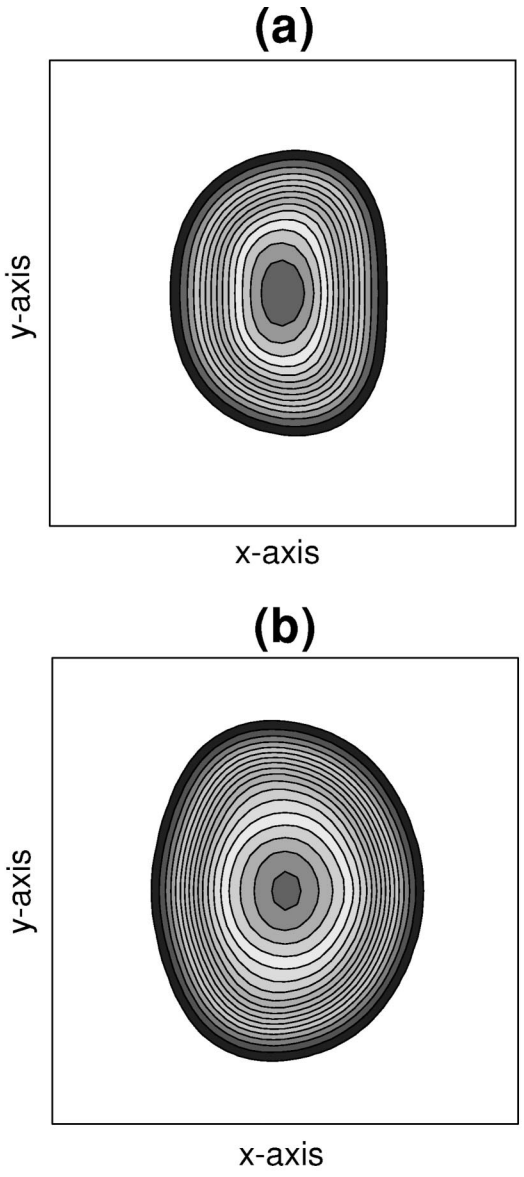

FIG. 5. The density distribution: (a) in the ND yrast band of ^{32}S at $\omega=2.2$ [MeV/$\hbar$]; (b) in the ND excited band of ^{56}Ni at $\omega=1.4$ [MeV/$\hbar$].

both in the proton and neutron fields. The labels of the most important orbits are given in Fig. 4(a) at $\omega=0$[MeV/$\hbar$]. Hereafter, the asymptotic Nilsson quantum numbers are used only for convenience, since they are not good quantum numbers when the reflection symmetry is absent. With the increase of the angular frequency the interaction between s.p. orbits associated with the principal quantum numbers $N=2$ and $N=3$, increases as well. In particular, the coupling between the orbit [330]1/2 and the [211]1/2 near the Fermi surface is essential for the mean field in the region $1.2\leqslant\omega\leqslant2.5$ [MeV/$\hbar$]. As a result, the Y_{31} deformation becomes favorable at $\omega\sim2.2$ [MeV/$\hbar$], for ^{32}S with a finite value $\beta_{31}=0.13$. The density distribution projected on the plane perpendicular to the rotation axis is shown in Fig. 5(a) for the yrast state at $\omega\sim2.2$ [MeV/$\hbar$] where the β_{31} deformation has a maximal value.

From the analysis of Figs. 3(a) and 6, it follows that there is a correlation between the behavior of the dynamical moment of inertia $\mathcal{J}^{(2)}(\omega)$ and the magnitude of the octupole deformation. Similar to the behavior of $|\beta_{31}|$, the dynamical moment of inertia $\mathcal{J}^{(2)}(\omega)$ begins to increase at $\omega\sim1.5$ [MeV/$\hbar$], and both quantities show local maxima around $\omega\sim2$ [MeV/$\hbar$]. Due to the strong octupole interaction, the quasicrossing between s.p. levels is smooth [Fig. 4(a)]. The static moment of inertia $\mathcal{J}^{(1)}(\omega)$ is less sensitive to the quasicrossing of s.p. levels and it changes smoothly with the increase of the rotational frequency ω. The quantity $\mathcal{J}^{(2)}(\omega)-\mathcal{J}_{\rm IB}$ nicely correlates with the change of the nonaxial octupole deformation $d\beta_{31}/d\omega$ for ^{32}S (see Fig. 6) caused by the rearrangement of the two-body interaction under the rotation. On the other hand, the IB moment of inertia also reflects the structural changes in the mean field similar to the dynamical moment of inertia $\mathcal{J}^{(2)}(\omega)$. It begins to increase at $\omega\sim1.5$ [MeV/$\hbar$] and shows a local maximum at $\omega\sim2.2$ [MeV/$\hbar$]. The correlation between the IB moment

of inertia and the magnitude of the octupole deformation $|\beta_{31}|$ may be understood within a simple two-level model described below.

Let us consider the situation when the high-lying intruder s.p. orbit μ is coming down to the highest last occupied orbit ν due to the Coriolis term $-\omega\hat{J}_z$. They have the same simplex quantum number. For the sake of simplicity, we restrict our discussion to the 2×2 subspace. We assume that (i) our states are eigenstates of the parity operator $\hat{P}$ at $\omega=0$ and (ii) there are no changes in the subspace expanded by the simplex partners of μ and ν at $\omega\neq 0$.

For $0\leqslant\omega\leqslant\omega_c$, the eigenstates can be written

$$\begin{pmatrix} |\nu(\omega)\rangle \\ |\mu(\omega)\rangle \end{pmatrix} = U \begin{pmatrix} |\nu(\omega=0)\rangle \\ |\mu(\omega=0)\rangle \end{pmatrix}$$

$$U=\begin{pmatrix} \cos\psi(\omega) & \sin\psi(\omega) \\ -\sin\psi(\omega) & \cos\psi(\omega) \end{pmatrix}, \tag{17}$$

where $|\psi(\omega)|$ is a monotonic function of ω.[1] The function $|\psi(\omega)|$ is defined such that (a) $0\leqslant|\psi(\omega)|\leqslant\pi/2$ and (b) $\psi(\omega=0)=0$, $|\psi(\omega_c)|=\pi/2$, where ω_c is the largest rotational frequency. Using the unitary transformation U, Eq. (17), one can find the density matrix

$$\boldsymbol{\rho}(\omega)=U\begin{pmatrix} 1 & 0 \\ 0 & 0 \end{pmatrix}U^{-1}$$

at $\omega\neq 0$. Taking into account that at $\omega=0$ the matrix elements of the octupole operator $\hat{Q}_3$ have the following structure

$$\boldsymbol{q}\equiv\begin{pmatrix} q_{\nu\nu} & q_{\nu\mu} \\ q_{\mu\nu} & q_{\mu\mu} \end{pmatrix}=\begin{pmatrix} 0 & q \\ q & 0 \end{pmatrix}, \tag{18}$$

where q is a finite real number, we obtain $|\langle\hat{Q}_3\rangle| = |\mathrm{tr}[\boldsymbol{q\rho}(\omega)]| = |q\sin 2\psi(\omega)|$, due to the assumption (ii). Since at $\omega=0$ matrix elements of the angular momentum operator $\hat{J}_z$ are defined as

$$\boldsymbol{j}\equiv\begin{pmatrix} j_{\nu\nu} & j_{\nu\mu} \\ j_{\mu\nu} & j_{\mu\mu} \end{pmatrix}=\begin{pmatrix} j & 0 \\ 0 & j' \end{pmatrix},$$

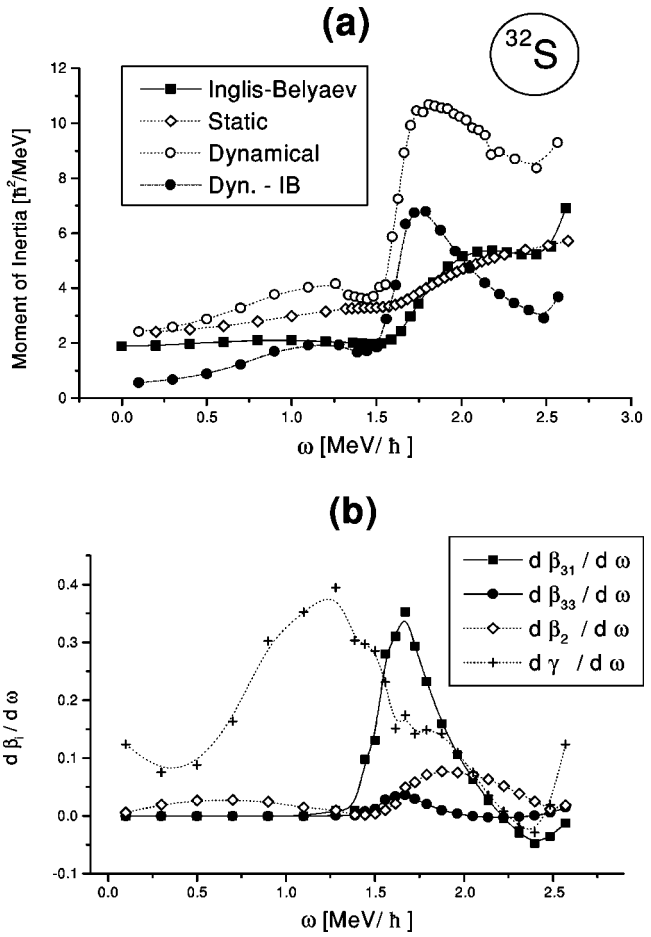

FIG. 6. The nucleus ^{32}S. On (a): the static, $\mathcal{J}^{(1)}(\omega)$ (open diamond), the dynamical, $\mathcal{J}^{(2)}(\omega)$ (open circle), the Inglis-Belyaev, $\mathcal{J}_{\mathrm{IB}}(\omega)$, (filled square) moments of inertia, and the difference $\mathcal{J}^{(2)}(\omega)-\mathcal{J}_{\mathrm{IB}}(\omega)$ (filled circle) versus the rotational frequency ω; on (b) the derivatives of deformations versus the rotational frequency: $d\beta_{31}/d\omega$ (filled square); $d\beta_{33}/d\omega$ (filled circle); $d\beta_2/d\omega$ (diamond); $d\gamma/d\omega$ (+). See the definition of different moments of inertia in the text.

using the unitary transformation U, Eq. (17), we obtain for the matrix elements of $\boldsymbol{j}$ at $\omega\neq 0$

$$\begin{pmatrix} j_{\nu\nu}(\omega) & j_{\nu\mu}(\omega) \\ j_{\mu\nu}(\omega) & j_{\mu\mu}(\omega) \end{pmatrix}=\begin{pmatrix} j\cos^2\psi(\omega)+j'\sin^2\psi(\omega) & (j'-j)\sin 2\psi(\omega)/2 \\ (j'-j)\sin 2\psi(\omega)/2 & j'\cos^2\psi(\omega)+j\sin^2\psi(\omega) \end{pmatrix}. \tag{19}$$

One can see that $|\langle\hat{Q}_3\rangle|$ and $|j_{\mu\nu}(\omega)|^2=(j'-j)^2\sin^2 2\psi(\omega)/4$ have a maximum at $|\psi(\omega)|=\pi/4$, where there is a strong mixing of the unperturbed eigenfunctions. Therefore, the $\mu\nu$ component of the Inglis-Belyaev moment of inertia

$$\frac{2|j_{\mu\nu}(\omega)|^2}{\epsilon_\mu(\omega)+\epsilon_\nu(\omega)}=\frac{(j'-j)^2\sin^2 2\psi(\omega)}{2[\epsilon_\mu(\omega)+\epsilon_\nu(\omega)]} \tag{20}$$

[1]A sign of $\psi(\omega)$ is not important for the absolute value of the octupole deformation.

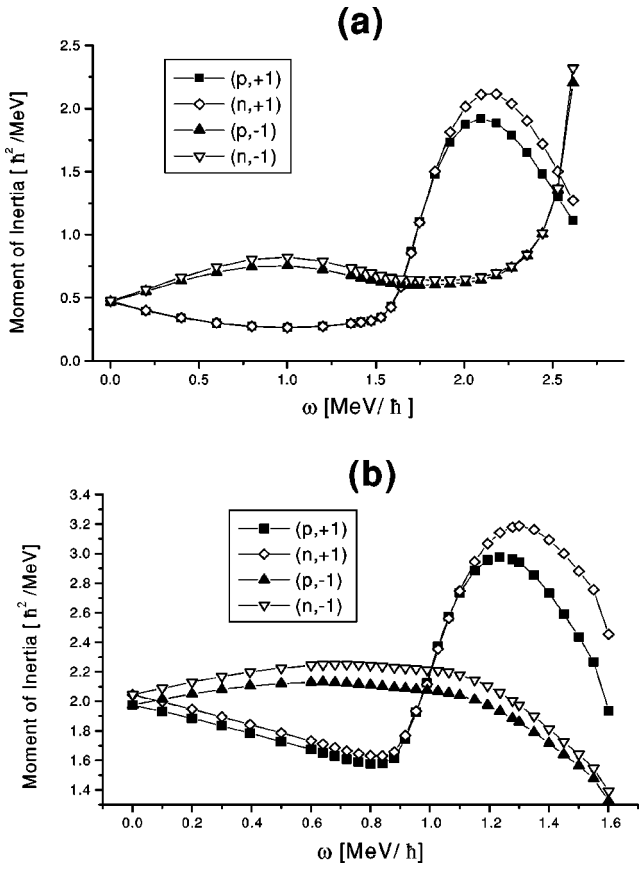

FIG. 7. Components of the Inglis-Belyaev, $\mathcal{J}_{\mathrm{IB}}(\omega)$, moment of inertia as a function of the rotational frequency ω: (a) in ^{32}S and (b) in ^{56}Ni. The notation of components is given in Eq. (15).

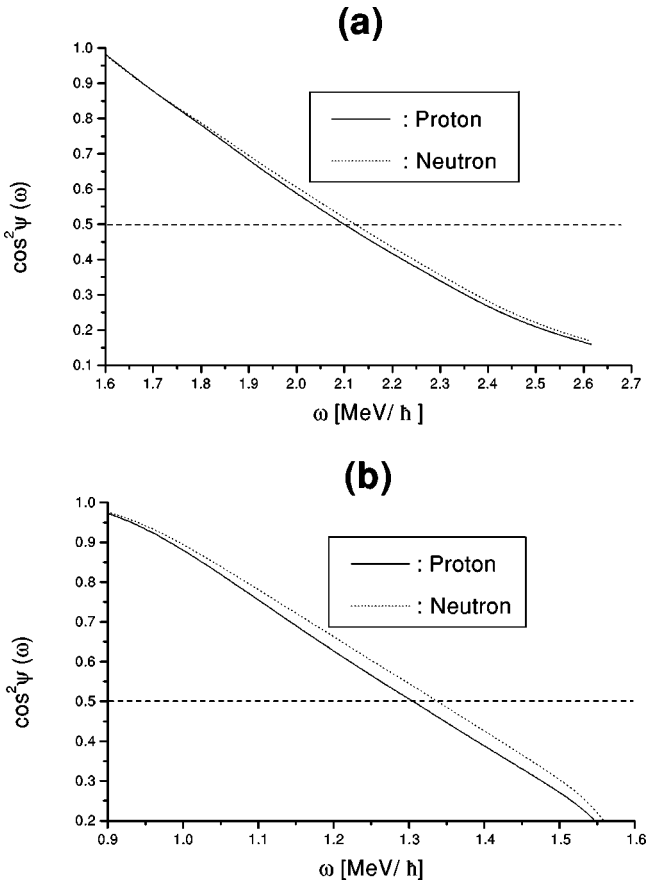

FIG. 8. The degree of mixing of intruder orbits, $\cos^2\psi(\omega)$, in the region of quasicrossing: (a) in ^{32}S and (b) in ^{56}Ni. The quantity $\cos^2\psi(\omega)$ is defined in the text.

may be large enough to affect the total value of the moment of inertia, because the denominator $\epsilon_\mu(\omega)+\epsilon_\nu(\omega)$ becomes small at this rotational frequency. Correspondingly, the two rotation-aligned single-particle states with a strong octupole coupling near the Fermi surface may give a large contribution to the value of the IB moment of inertia.

From Fig. 7(a), it follows that the magnitudes of $\mathcal{J}_{p,+1}(\omega)$ and $\mathcal{J}_{n,+1}(\omega)$ [see Eq. (15)] are smaller than those from the $s=-1$ subspaces which play dominant roles in the collective rotation at low spins, in the region $\omega<1.5$ [MeV/$\hbar$]. However, for $\omega>1.5$ [MeV/$\hbar$], $\mathcal{J}_{p,+1}(\omega)$ and $\mathcal{J}_{n,+1}(\omega)$ begin to increase rapidly and they show local maxima at $\omega\sim2.2$ [MeV/$\hbar$] where $|\beta_{31}|$ also shows the maximum. Since $\mathcal{J}_{p,-1}(\omega)$ and $\mathcal{J}_{n,-1}(\omega)$ are almost unchanged in this region, the Y_{31} deformation occurs mainly due to the s.p. quasicrossing in the $s=+1$ subspaces. To justify this statement we calculate the quantity $\cos^2\psi(\omega)$. Using the identity of the intruder orbits μ which have odd parity at $\omega=0$[MeV/$\hbar$], we evaluate the $\cos^2\psi(\omega)$ approximately as

$$\cos^2\psi(\omega)\approx\sum_{n_x+n_y+n_z=odd}|\langle n_x,n_y,n_z;\sigma|\mu(\omega)\rangle|^2, \tag{21}$$

where a s.p. vector $|n_x,n_y,n_z;\sigma\rangle$ is a component of the Goodman basis in the $s=+1$ subspace and n_x, n_y, and n_z are the number of quanta on the x, y, and z axes, respectively. As is shown in Fig. 8(a), the evaluated value of $\cos^2\psi(\omega)=1/2$ or equivalently $|\psi(\omega)|=\pi/4$ at $\omega\sim2.2$ [MeV/$\hbar$]. Within the two-level model at this value of $|\psi(\omega)|$, the mixing of s.p. states with opposite parities is the strongest one.

Similar to the results in Ref. [17], our calculations show rather shallow minima for the β_{31} deformation [see Fig. 9(a)]. The contribution of the ground state octupole correlations may improve the mean field prediction. For example, recent analysis [44,45] clearly demonstrates the improvement of the mean field results by taking into account the correlations caused by the pairing vibrations. The contribution of octupole vibrations may be estimated in the random phase approximation as is given in [46] according to the prescription [47].

As is seen in Fig. 6(a), both the moments of inertia, $\mathcal{J}^{(2)}(\omega)$ and $\mathcal{J}_{\mathrm{IB}}(\omega)$, begin to increase again at $\omega\sim2.5$ [MeV/$\hbar$]. This is apparently due to the quasicrossings in the $s=-1$ subspaces at this point. There are also level-crossings between s.p. orbits with different simplex numbers [Fig. 4(a)], which suggest the instability of the z-simplex symmetrized state at high spins. We may speculate that the breaking of the z-simplex symmetry due to the tilted or the chiral rotation [10] may lead to a better description of high spin states in ^{32}S at $\omega\geqslant2.5$ [MeV/$\hbar$].

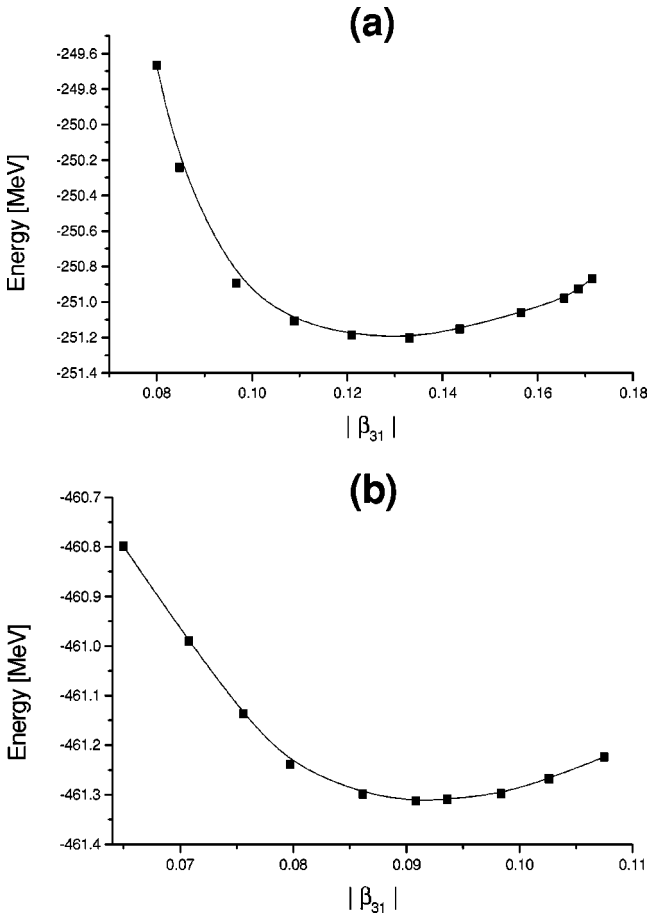

FIG. 9. The potential energy curve along the β_{31} direction: (a) in ^{32}S at $\omega=2.2$ [MeV/$\hbar$] and (b) in ^{56}Ni at $\omega=1.4$ [Mev/$\hbar$]. The calculated values of the β_{31} indicated by symbols are connected by a solid line.

B. ^{56}Ni

Our calculations reproduce the binding energies and the charge radii of ground states in $^{56-60}$Ni quite well. In this chain, which includes closed and open shell nuclei, we concentrate our attention on ^{56}Ni.

Though the shape of the ground state in ^{56}Ni is spherical, we also found two shape isomers with the ND and SD configuration at $\omega=0$ [MeV/$\hbar$], which are $\sim$5 MeV and $\sim$18 MeV above the ground state, respectively (see Fig. 10). The yrast nonrotating states observed in ^{56}Ni are related to vibrational excitations. In fact, their properties can be studied within the self-consistent cranking approach with the rotation *around a symmetry axis* [50] and we will discuss this subject in a forthcoming paper. The calculations for the ground state, ND and SD bands have been done in a manner similar to those of ^{32}S in the HF approximation, since the contribution of the pairing interaction terms to the total binding energies are almost negligible. At low spins the SD minimum is formed by the $4p$-$4h$ configuration $\pi[(3)^{-2}(4)^2]\nu[(3)^{-2}(4)^2]$ with respect to the ground state in ^{56}Ni. This SD configuration has a prolate shape with the quadrupole deformation $\beta_2=0.6$ (Fig. 2). It is also $4h$ configuration with respect to the SD state in ^{60}Zn due to the $N=30$ SD gap in the Zn isotopes [51], which is also seen in Fig. 11. The macroscopic-microscopic calculations [52,53] also predict the SD shape at large rotational frequencies. We restricted our analysis of the SD band, however, to the region of $\omega=0.0-0.4$ [MeV/$\hbar$], since at larger rotational frequencies the contribution of higher shells ($N>10$) becomes important.

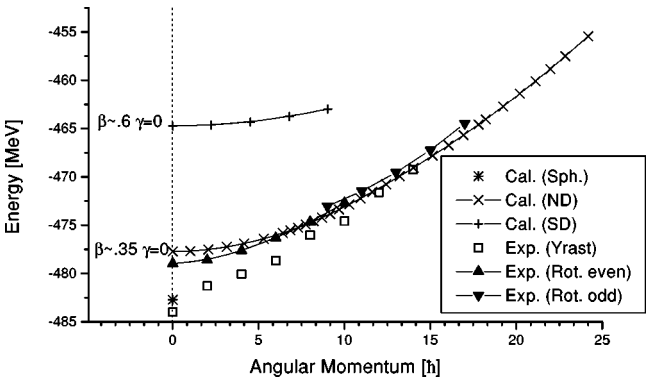

FIG. 10. The total binding energy in ^{56}Ni as a function of the angular momentum. The calculated points indicated by symbols + and $\times$ for SD and ND states, respectively, are connected by solid lines. The values of the quadrupole deformations β_2 and γ are given for each band at $I=0$. Experimental values for different states are indicated by symbols: open square is used for the yrast states; filled triangle up is used for rotational states with even spins; filled triangle down is used for rotational states with odd spins. Experimental values of the total binding energy, excited levels, and rotational states are from Refs. [39,48,49], respectively.

By using the decomposition of the axial harmonic oscillator into the isotropic ones, the relation between multiclusters and mean field results has been discussed in Ref. [54]. For SD shapes in the axial harmonic oscillator, one symmetric and one asymmetric combinations of spherical oscillators are expected (see also Ref. [12]). Within this model the SD states in ^{56}Ni should correspond to the asymmetric combination of two spherical oscillators with magic numbers 40 and 16. The density distribution brought about by the Gogny interaction for the SD state (see Fig. 12) does

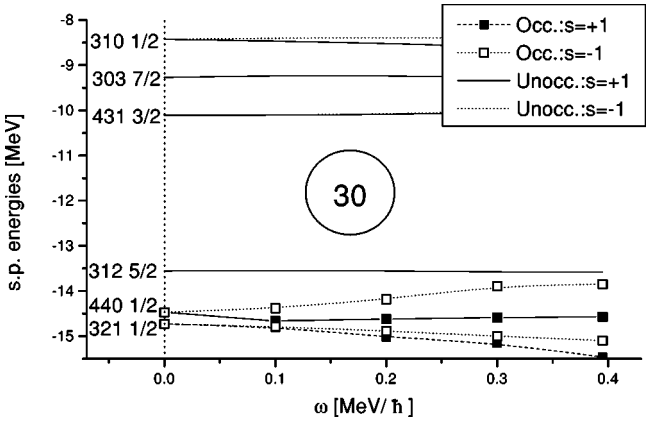

FIG. 11. Neutron single-particle energies of ^{56}Ni along the SD band near the Fermi surface. The symbols used here are defined in Fig. 4.

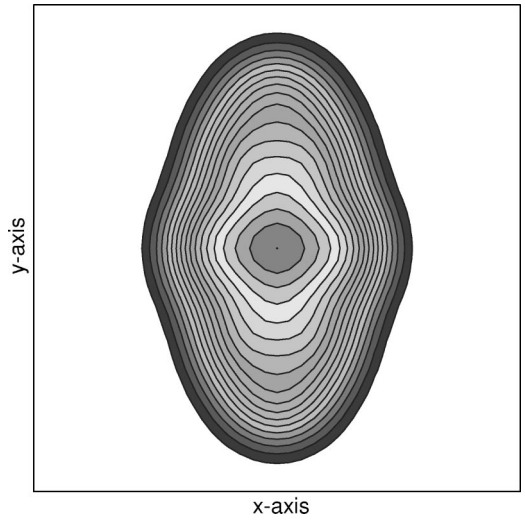

FIG. 12. The density distribution of the SD minimum at $\omega=0$ [MeV/$\hbar$] in ^{56}Ni.

not show such a multicluster structure at $\omega=0$ [MeV/$\hbar$]. Our configuration space is too small for us to reach a definite conclusion. On the other hand, the harmonic oscillator is useful only for predicting a general tendency towards mass asymmetry, for a certain particle number for SD shapes. Notice that the SD minimum could be related to the resonance state in the ^{28}Si+^{28}Si collision at high excitation energy $E^*_{\rm c.m.}=65$–70 MeV and high angular momenta $I=34$–$42\,\hbar$, as reported in Refs. [55–57]. A thorough study of ^{56}Ni as well as of ^{32}S at high spins may help to understand the link between the tendency for nuclei to create strongly deformed shapes and the tendency to develop the cluster structure.

A prolate deformation $\beta_2=0.35$ is found for the ND minimum at $\omega=0.0$ [MeV/$\hbar$] (Fig. 2). As is seen in Fig. 10, the calculated energies agree well with experimental data [48]. In many details, our results are similar to the ones obtained in the calculations based on the shell model and the HF(B)+ Skyrme forces [48]. In addition, in our calculations the nonaxial octupole deformation Y_{31} arises in the ND band with the increase of the rotational frequency. As is seen in Fig. 3(b), the value of the nonaxial octupole deformation increases rapidly around $\omega\sim0.9$ [MeV/$\hbar$]. It corresponds to $I\sim10[\hbar]$, where the pseudo-level-crossing occurs between s.p. orbits with the principal quantum numbers $N=3$ and $N=4$ [Fig. 4(b)]. A coupling between the [440]1/2 orbit and the [321]1/2 orbit take place near the Fermi surface in the region $0.8\leqslant\omega\leqslant1.6$ [MeV/$\hbar$]. The maximal value of the Y_{31} deformation, $\beta_{31}=0.09$, is approached at $\omega\sim1.4$ [MeV/$\hbar$] [Fig. 3(b)]. As is seen in Fig. 7(b), $\mathcal{J}_{p,+1}(\omega)$ and $\mathcal{J}_{n,+1}(\omega)$ increase rapidly around $\omega\sim0.9$ [MeV/$\hbar$] and approach the maximal value at $\omega\sim1.3$ [MeV/$\hbar$]. Using the two-level model and similar arguments as for the case of ^{32}S, we may conclude the following: – since $\mathcal{J}_{p,-1}(\omega)$ and $\mathcal{J}_{n,-1}(\omega)$ are decreasing in this region of the rotational frequency, it is most likely that the octupole deformation is caused by the quasicrossing of s.p. levels in the $s=+1$ subspaces. The function $\cos^2\psi(\omega)$ of the intruder orbits with the positive

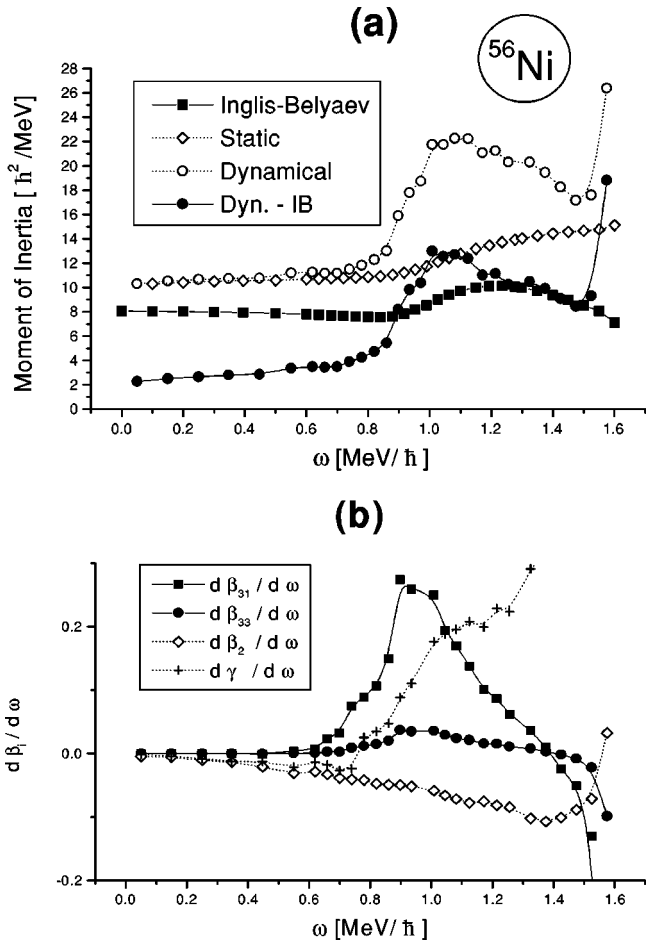

FIG. 13. The nucleus ^{56}Ni. The symbols used here are defined in Fig. 6.

parity at $\omega=0$ [MeV/$\hbar$] for both the proton and neutron fields,

$$\cos^2\psi(\omega)\approx\sum_{n_x+n_y+n_z=even}|\langle n_x,n_y,n_z;\sigma|\mu(\omega)\rangle|^2, \tag{22}$$

have maximal values at $\omega\sim1.3$ [MeV/$\hbar$] and $\omega\sim1.35$ [MeV/$\hbar$], where the components of the IB moment of inertia, $\mathcal{J}_{p,s=+1}(\omega)$ and $\mathcal{J}_{n,s=+1}(\omega)$, show maxima, respectively [Fig. 8 (b)].

The dynamical and IB moments of inertia also increase at $\omega\sim0.9$ [MeV/$\hbar$] and exhibit maxima around $\omega\sim1.2$ [MeV/$\hbar$] (Fig. 13). It is slightly different from the result [48] predicting the maximum of $\mathcal{J}^{(2)}$ at $\omega\sim1.5$ [MeV/$\hbar$]. Similar to the case of ^{32}S, there is a correspondence between the behavior of quantity $\mathcal{J}^{(2)}(\omega)-\mathcal{J}_{\rm IB}$ and the evolution of the octupole deformation of the self-consistent mean field with the rotation and the maximum in $\mathcal{J}^{(2)}$ is correlated with the maximum of $d\beta_{31}/d\omega$. However, the behavior of the $\mathcal{J}^{(2)}(\omega)$ and $\mathcal{J}_{\rm IB}(\omega)$ moment of inertia is less correlated at larger values of the rotational frequency. The pseudocrossing is much sharper in ^{56}Ni in comparison with the one in ^{32}S (Fig. 4), i.e., the octupole interaction is expected to be

weaker. The function $\cos^2\psi(\omega)$ for both the fields decreases rapidly at $\omega > 1.55$ [MeV/$\hbar$] [see Fig. 8(b)]. Due to the termination of the parity mixing of the s.p. levels, the matrix element $J_{ij}(\omega)$ between mixed states, given by Eq. (12), falls rapidly. As a result, the IB moment of inertia, $\mathcal{J}_{\rm IB}(\omega)$, also decreases. On the other hand, the dynamical moment of inertia, $\mathcal{J}^{(2)}(\omega)$, reflects variations of the self-consistent mean field. In particular, the changes of the γ and β_2 deformations, $d\beta_2/d\omega$ and $d\gamma/d\omega$, give rise to the change of the $\mathcal{J}^{(2)}(\omega)$. A quadrupole interaction leads to the quasicrossing between occupied levels [321]1/2 and [312]5/2 and causes the increase of the $\mathcal{J}^{(2)}(\omega)$ as well. Due to the rearrangement of the two-body interaction under the rotation, the high intruder unoccupied state ($s=+$) contributes to the sudden increase of the dynamical moment of inertia observed at high rotational frequencies $\omega > 1.5$ [MeV/$\hbar$]. Finally, we note that the octupole minimum in ^{56}Ni is much more shallow in comparison with the one in ^{32}S [Fig. 9(b)].

IV. SUMMARY

It was expected from various calculations based on the macroscopic-microscopic method that octupole deformations would arise in rotating nuclei [3]. Using the cranking HF(B) approach with the effective Gogny interaction, we found that the nonaxial octupole deformation associated with the Y_{31} term in the octupole family becomes important in the yrast band of ^{32}S at the angular momenta $I \geqslant 5[\hbar]$. The primary mechanism behind the occurrence of the octupole deformation is related to the strong mixing via octupole interaction of s.p. orbits with a positive simplex quantum number. Similar phenomena have been observed in the nucleus ^{56}Ni, where we predict the octupole softness in the excited ND band at high spins $I \geqslant 10[\hbar]$.

In conclusion, an exploration of the octupole phenomenon certainly could deepen our understanding of different aspects of the spontaneous symmetry breaking mechanism in finite Fermi systems like nuclei. In particular, the breaking of the intrinsic reflection symmetry could be related to unexpected strong electric dipole and octupole transitions in rotational bands and to a formation of multicluster structures in strongly deformed nuclei. It seems that the nonaxial octupole deformations may often accompany the onset of the superdeformation. The results for ^{32}S support this idea. Furthermore, shell effects caused by the nonaxial octupole deformations in combination with normal quadrupole deformations mimic the superdeformed shell structure [21]. Measurements with new generations of modern detectors could test the predictions made within the HF(B) approach and lead to new insights regarding effective nucleon-nucleon interactions and their properties.

ACKNOWLEDGMENTS

We are thankful to F. Sakata, Y. Hashimoto, and Y. Kanada-En'yo for their support in numerical calculations. We are also grateful to K. Matsuyanagi for illuminating communications. We appreciate discussions with A. Titov and A. Wagner. This work was supported in part by the Russian Foundation for Basic Research under Grant No. 00-02-17194.

[1] A. Bohr and B. Mottelson, *Nuclear Structure*, Vol. 2 (Benjamin, New York, 1975).
[2] P. Ring and P. Schuck, *The Nuclear Many-Body Problem* (Springer-Verlag, Berlin, 1980).
[3] S. Åberg, H. Flocard, and W. Nazarewicz, Annu. Rev. Nucl. Part. Sci. **40**, 439 (1990).
[4] Z. Patyk, A. Baran, J.F. Berger, J. Dechargé, J. Dobaczewski, P. Ring, and A. Sobiczewski, Phys. Rev. C **59**, 704 (1999).
[5] P.J. Nolan and P.J. Twin, Annu. Rev. Nucl. Part. Sci. **38**, 533 (1988).
[6] R.V.F. Janssens and T.L. Khoo, Annu. Rev. Nucl. Part. Sci. **41**, 321 (1991).
[7] C. Baktash, B. Haas, and W. Nazarewicz, Annu. Rev. Nucl. Part. Sci. **45**, 485 (1995).
[8] C. Baktash, Prog. Part. Nucl. Phys. **38**, 291 (1997).
[9] P.A. Butler and W. Nazarewicz, Rev. Mod. Phys. **68**, 349 (1996).
[10] S. Frauendorf, Rev. Mod. Phys. (submitted).
[11] T. Nakatsukasa, K. Matsuyanagi, and S. Mizutori, Prog. Theor. Phys. **87**, 607 (1992).
[12] R. Nazmitdinov and S. Åberg, Phys. Lett. B **289**, 238 (1992).
[13] J. Skalski, P.-H. Heenen, P. Bonche, H. Flocard, and J. Meyer, Nucl. Phys. **A551**, 109 (1993).
[14] R.R. Chasman, Phys. Lett. B **266**, 243 (1991).
[15] X. Li and J. Dudek, Phys. Rev. C **49**, R1250 (1994).
[16] S. Takami, K. Yabana, and M. Matsuo, Phys. Lett. B **431**, 242 (1998).
[17] M. Yamagami and K. Matsuyanagi, Nucl. Phys. **A672**, 123 (2000).
[18] W.D. Heiss, R.G. Nazmitdinov, and S. Radu, Phys. Rev. Lett. **72**, 2351 (1994); Phys. Rev. B **51**, 1874 (1994); Phys. Rev. C **52**, 3032 (1995).
[19] A. Arita and K. Matsuyanagi, Prog. Theor. Phys. **91**, 723 (1994); Nucl. Phys. **A592**, 9 (1995).
[20] W.D. Heiss, R.A. Lynch, and R.G. Nazmitdinov, JETP Lett. **69**, 563 (1998).
[21] W.D. Heiss, R.A. Lynch, and R.G. Nazmitdinov, Phys. Rev. C **60**, 034303 (1999).
[22] D. Gogny, in *Nuclear Self-Consistent Fields*, edited by G. Ripka and M. Porneuf (North-Holland, Amsterdam, 1973), p. 333.
[23] J. Dechargé and D. Gogny, Phys. Rev. C **21**, 1568 (1980).
[24] M. Girod and B. Grammaticos, Phys. Rev. C **27**, 2317 (1983).
[25] J.F. Berger, M. Girod, and D. Gogny, Nucl. Phys. **A428**, 23c (1984); **A502**, 85c (1989); Comput. Phys. Commun. **63**, 365 (1991).
[26] J.L. Egido and L.M. Robledo, Phys. Rev. Lett. **70**, 2876 (1993); J.L. Egido, L.M. Robledo, and R.R. Chasman, Phys. Lett. B **322**, 22 (1994).
[27] M. Girod, J.P. Delaroche, J.F. Berger, and J. Libert, Phys. Lett. B **325**, 1 (1994).

[28] E. Caurier, J.L. Egido, G. Martínez-Pinedo, A. Poves, J. Retamosa, L.M. Robledo, and A.P. Zuker, Phys. Rev. Lett. **75**, 2466 (1995); G. Martínez-Pinedo, A. Poves, L.M. Robledo, E. Caurier, F. Nowacki, J. Retamosa, and A.P. Zuker, Phys. Rev. C **54**, R2150 (1996); S.M. Lenzi *et al.*, *ibid.* **56**, 1313 (1997).
[29] T. Tanaka, F. Sakata, and K. Iwasawa, Phys. Rev. C **58**, 2765 (1998).
[30] T. Tanaka, F. Sakata, T. Marumori, and K. Iwasawa, Phys. Rev. C **56**, 180 (1997).
[31] K. Iwasawa, F. Sakata, T. Tanaka, Y. Hashimoto, and T. Marumori, *Progress in Particle and Nuclear Physics* (Elsevier Science, New York, 1997), Vol. 38, p. 249.
[32] J. Dobaczewski, J. Dudek, S.G. Rohozinski, and T.R. Werner, Phys. Rev. C **62**, 014310 (2000); **62**, 014311 (2000).
[33] H. Flocard, P. Quentin, A.K. Kerman, and D. Vautherin, Nucl. Phys. **A203**, 433 (1973).
[34] A.L. Goodman, in *Advances in Nuclear Physics*, edited by J.W. Negele and E. Vogt (Plenum, New York, 1979), Vol. 11, p. 293.
[35] S.T. Belyaev, in *Selected Topics in Nuclear Theory*, edited by F. Janouch (IAEA, Vienna, 1963), p. 291; Nucl. Phys. **24**, 322 (1961).
[36] A.B. Migdal, Nucl. Phys. **13**, 655 (1959).
[37] I. Hamamoto, Nucl. Phys. **A232**, 445 (1974); J. Helgesson and I. Hamamoto, Phys. Scr. **40**, 595 (1989); I. Hamamoto and W. Nazarewicz, Phys. Rev. C **49**, 2489 (1994).
[38] D.J. Thouless and J.G. Valatin, Nucl. Phys. **31**, 211 (1962).
[39] G. Audi and A.H. Wapstra, Nucl. Phys. **A565**, 1 (1993).
[40] P.M. Endt, Nucl. Phys. **A521**, 1 (1990).
[41] R.R. Rodriguez-Guzman, J.L. Egido, and L.M. Robledo, Phys. Rev. C **62**, 054308 (2000).
[42] M. Anguiano, J.L. Egido, and L.M. Robledo, nucl-th/0008055.
[43] H. Molique, J. Dobaczewski, and J. Dudek, Phys. Rev. C **61**, 044304 (2000).
[44] D. Almehed, F. Dönau, S. Frauendorf, and R.G. Nazmitdinov, Phys. Scr. **T88**, 62 (2000); D. Almehed, S. Frauendorf, and F. Dönau, nucl-th/9901070, v.2.
[45] K. Hagino and G.F. Bertsch, Phys. Rev. C **61**, 024307 (2000); Nucl. Phys. **A679**, 163 (2000).
[46] J. Kvasil and R.G. Nazmitdinov, Nucl. Phys. **A439**, 86 (1985).
[47] F. Dönau, D. Almehed, and R.G. Nazmitdinov, Phys. Rev. Lett. **83**, 280 (1999).
[48] D. Rudolph *et al.*, Phys. Rev. Lett. **82**, 3763 (1999).
[49] H. Junde, Nucl. Data Sheets **67**, 523 (1992).
[50] E.R. Marshalek and R.G. Nazmitdinov, Phys. Lett. B **300**, 199 (1993); E.R. Marshalek, R.G. Nazmitdinov, and I. Ragnarsson, Bull. Russ. Acad. Sci. Phys. **57**, 1709 (1993).
[51] C.E. Svensson *et al.*, Phys. Rev. Lett. **79**, 1233 (1997); **82**, 3400 (1999); M. Devlin *et al.*, *ibid.* **82**, 1233 (1999).
[52] R.K. Sheline, I. Ragnarsson, and S.G. Nilsson, Phys. Lett. **41B**, 115 (1972).
[53] T. Bengtsson, M. Faber, M. Ploszajczak, I. Ragnarsson, and S. Åberg, Lund-MPh-84/01.
[54] W. Nazarewicz and J. Dobaczewski, Phys. Rev. Lett. **68**, 154 (1992).
[55] R.R. Betts *et al.*, Phys. Rev. Lett. **47**, 23 (1981); R.R. Betts, Nucl. Phys. **A447**, 257c (1985).
[56] E. Uegaki and Y. Abe, Phys. Lett. B **340**, 143 (1994).
[57] R. Nouicer *et al.*, Phys. Rev. C **60**, 041303(R) (1999).